Correlation between Slag Reactivity and Cement Paste Properties
The Influence of Slag Chemistry

Zhang, Yu; Çopuroğlu, Oğuzhan

DOI
10.1061/JMCEE7.MTENG-16385
Publication date
2023
Document Version
Final published version
Published in
Journal of Materials in Civil Engineering

Citation (APA)
Zhang, Y., & Çopuroğlu, O. (2023). Correlation between Slag Reactivity and Cement Paste Properties: The Influence of Slag Chemistry. *Journal of Materials in Civil Engineering*, *36*(3), Article 04023618. https://doi.org/10.1061/JMCEE7.MTENG-16385

Correlation between Slag Reactivity and Cement Paste Properties: The Influence of Slag Chemistry

Yu Zhang, Ph.D.[1]; and Oğuzhan Çopuroğlu[2]

Abstract: The properties of slag-rich cement paste are fundamentally associated with slag chemistry. In the present research, 10 slags covering the common chemistry range, including eight synthetic slags of $CaO—SiO_2—Al_2O_3—MgO$ system and two commercial slags, were adopted to evaluate the influence of slag composition on the early (7 days) and later (3 months) age properties of blended paste. Mixture containing Al_2O_3-rich slag performed better at 7 days as it favored the formation of ettringite and/or monosulfate. The MgO-rich slag cement paste exhibited good properties at both early and later ages, and it effectively promoted the precipitation of Mg-Al hydrotalcite-like phase. It was also noted that the Mg/Al atomic ratio of hydrotalcite-like phase was positively related to the Mg/Al atomic ratio of slag itself. Conversely, with the increasing MgO content in slag, the Al/Si atomic ratio of C—S(A)—H gel phase decreased. High Al_2O_3 and/or MgO contents can compensate the negative effect of reduced CaO/SiO_2 ratio at early age while not at later age. Overall, attention should be paid to aluminum- and sulfur-rich slags. These two elements in slag promoted the formation of ettringite and/or monosulfate at an early age; however, this positive effect disappeared at later ages. **DOI:** 10.1061/JMCEE7.MTENG-16385. © *2023 American Society of Civil Engineers.*

Author keywords: Synthetic slag; Slag-rich cement paste; Early- and late-age properties; Al_2O_3 and MgO; Graphic method.

Introduction

Blast furnace slag, which will be referred to as slag in this paper is the waste of producing pig iron. The raw iron ore gangue, reduced substances, and components of melted coke are mixed together in the blast furnace to form liquid slag at a temperature of around 1,450°C (Yang et al. 2014). Its major constituents, calcium oxide and silica, are present in large quantities. Also, slag contains significant amounts of minor components, i.e., alumina and magnesia. Thus, it is commonly described as a $CaO—SiO_2—Al_2O_3—MgO$ quaternary system. Additionally, slag absorbs neighboring alkalis like Na and K as well as sulfur compounds, as trace constituents (Sohn and Min 2012). Through rapid cooling with powerful water jets, molten slag solidifies immediately and turns into a granular and almost fully glassy form, also called as granulated slag. In most cases, slag is employed as a kind of supplementary cementitious material for cement and concrete productions (Juenger et al. 2019; Li et al. 2016; Özbay et al. 2016).

To produce strength-building hydration products, latent hydraulic slag needs to be stimulated, which is different from hydraulic binders that can react with water, e.g., ordinary portland cement. The stimulator can be NaOH/water glass solution found in alkali-activated slag paste or portlandite, which is generated as ordinary portland cement hydrates and therefore is available in slag-containing cement paste. For cement clinker, the hydration products consist primarily of calcium silicate hydrates (C—S—H gel phase), portlandite, ettringite, and calcium monosulfoaluminate (monosulfate in short) (Taylor 1997). As for the hydrates of slag, secondary precipitations including calcium silicate hydrates and Mg-Al hydrotalcite-like phase have been discovered (Chen and Brouwers 2007; Taylor et al. 2010; Zhang et al. 2022a, c).

In a previous study (Zhang et al. 2022d), hydraulicity test (R3 test) based on a simplified mixture and dissolution test in a NaOH solution were utilized to study the correlation between slag chemistry and reactivity. Meanwhile, a new perspective using novel graphical approach was put forward to classify slag reactivity based on its four main components. As revealed in the research, high Al_2O_3 and/or MgO contents in slag commonly resulted in high reactivity, and it can even compensate the adverse effect of reduced CaO/SiO_2 ratio. These outputs were consistent with results found by Bougara et al. (2010), Kucharczyk et al. (2019), and Schöler et al. (2017). However, some researchers pointed out that slag reactivity indicated by these rapid and simplified measurements (e.g., R3 test, Chapelle test, Frattini test) was more related to the early age properties of blended system (Blotevogel et al. 2020). Especially for alumina-rich slag, increased Al_2O_3 content was reported to enhance the production of Al-containing phases, e.g., ettringite and monosulfate. Due to their higher molar volume, they can fill up pores and are beneficial for early age strength development (Whittaker et al. 2014). At the same time, systematic investigations concerning the interaction among slag chemistry, reactivity, and later age properties of slag cement paste were still scarce.

Based on the results of Zhang et al. (2022d), 10 slags covering the common chemistry range, including eight synthetic slags and two commercial slags, were utilized in the current study. Both early age (7 days) and later age (3 months) properties of slag-rich cement paste were estimated by different characterization methods. To obtain compressive strength, test was carried out in compliance to the standard EN 196-1 (CEN 2016). A TAM Air isothermal calorimeter was used to measure the heat evolution profile of each mixture until 7 days. Besides, thermogravimetric (TG), X-ray diffraction (XRD),

---

[1] Key Laboratory of Concrete and Prestressed Concrete Structures of the Ministry of Education, Southeast Univ., Nanjing 210096, China (corresponding author). ORCID: https://orcid.org/0000-0003-4668-1553. Email: 101013462@seu.edu.cn

[2] Associate Professor, Microlab, Section Materials and Environment, Faculty of Civil Engineering and Geosciences, Delft Univ. of Technology, Delft 2628 CN, Netherlands. Email: O.Copuroglu@tudelft.nl

Note. This manuscript was submitted on January 29, 2023; approved on August 28, 2023; published online on December 27, 2023. Discussion period open until May 27, 2024; separate discussions must be submitted for individual papers. This paper is part of the ***Journal of Materials in Civil Engineering***, © ASCE, ISSN 0899-1561.

J. Mater. Civ. Eng., 2024, 36(3): 04023618

and environmental scanning electron microscopy (ESEM) were adopted to examine the phase assemblage of each hydrated specimen. The distribution of pores was analyzed using mercury intrusion porosimetry (MIP). Moreover, the graphical approach proposed in Zhang et al. (2022d) was further employed to evaluate the interaction among the properties of slag-rich cement paste, slag chemistry, and reactivity at both early (7 days) and later (3 months) ages.

Materials and Methodology

Materials

The CEM I 42.5 N utilized in the present study was purchased from ENCI Maastricht B.V. Eight synthetic slags produced in the laboratory and two commercial slags collected from iron/steel manufacturing factory (provided by Ecocem Benelux B.V.) were adopted to produce the cement-slag system. Quartz (Qz) was also introduced to cast the cement-quartz paste and act as a reference. Readers can refer to Zhang et al. (2022d) for the detailed production process of eight synthetic slags.

The chemical composition of raw materials is presented in Table 1. For synthetic Slags M0, M8, and M16, the MgO content was increased from 0.33% to 16.07% by weight. As for synthetic Slags A3, A12, and A18, the amount of Al_2O_3 was in the range of 3.69%–18.19% by weight. The CaO/SiO_2 ratio of synthetic slag CS1 and CS2 was 0.85 and 0.65, respectively, both of which were less than 1. Note that the chemical composition of commercial Slags S1 and S2 was similar to that of synthetic Slag M8. Table 2 reports the mineralogical composition of CEM I 42.5 N according to Bouge calculation. Fig. 1 displays the particle size distribution of slag and quartz. As can be seen, synthetic slags and quartz exhibited a similar d_{50} at approximately 20 μm.

For each mixture design, 70% by weight cement was substituted by synthetic slag or quartz, and the water to binder (cement plus synthetic slag/quartz) ratio was kept at 0.4. Paste specimens of $20 \times 20 \times 20$ mm cube were prepared for further analysis, all of which were packed in sealed plastic bags and kept at ambient temperature. For each testing age (7, 28, and 90 days), an individual sample was prepared.

Methodology

For heat evolution of each blended mixture, it was measured using a TAM Air isothermal calorimeter at 20°C over the course of 7 days. A total of ~7 g mixed materials (5 g binder + 2 g water) of each group was weighted, put in glass ampoules, and transported to the calorimeter for evaluating. As for compressive strength test, five paste cubes of each mixture were measured at each time step, following the procedure described in the standard EN 196-1.

For XRD, specimens were crushed, and the selected slices were placed in isopropanol solution to extract free water. After drying, they were ground and sieved manually to obtain fine powders (<63 μm). A Philips Powder Diffractometer PW 1830/40 with Cu K-alpha radiation was used to collect XRD data. Powders were scanned from 5° to 60° (2θ) at an acceleration voltage of 40 kV and an X-ray beam current of 40 mA, with a step size of 0.03°. As for TG analysis, Netzsch STA 449 F3 Jupiter coupled with mass spectrometer (MS) Netzsch QMS 430 C was employed. Approximately 50 mg sample powder was heated from 40°C to 900°C (10°C/min) under an argon atmosphere.

Following the steps introduced in Kocaba et al. (2012), the mixture solution of sodium carbonate, ethylenediaminetetraacetic acid (EDTA), and triethanolamine was adopted to determine the reaction

Table 2. Mineralogical composition of CEM I 42.5 N based on Bouge calculation

Phase	% by weight
C_3S	62.24
β-C_2S	10.47
C_3A	8.18
C_4AF	9.12
Gypsum	4.98
Other	5.01

Table 1. Chemical composition (% by weight) determined by X-ray fluorescence (XRF) and physical properties of cement and slags

Component	Cement	M0	M8	M16	A3	A12	A18	CS1	CS2	S1	S2
CaO	64	43.16	37.04	34.09	42.07	37.32	36.87	**32.98**	**28.05**	39.91	37.40
SiO_2	20	42.99	37.79	32.99	43.30	39.11	34.43	**38.67**	**42.84**	38.79	37.82
Al_2O_3	5	13.30	14.51	15.05	**3.69**	**12.32**	**18.19**	14.51	17.12	10.94	13.58
MgO	—	**0.33**	**8.83**	**16.07**	10.83	9.43	7.98	11.22	9.67	6.82	8.11
FeO/Fe_2O_3	3	0.07	0.28	0.34	0.07	0.30	0.40	0.36	0.35	0.31	0.36
TiO_2	—	—	0.70	0.73	—	0.70	0.84	1.02	0.89	0.77	1.22
MnO/Mn_2O_3	—	—	0.17	0.16	—	0.15	0.27	0.22	0.19	0.21	0.30
Na_2O	0.58	—	0.24	0.22	—	0.24	0.37	0.36	0.31	0.42	—
K_2O	—	—	0.25	0.21	—	0.21	0.41	0.36	0.32	0.27	0.8
SO_3	2.93	0.01	0.01	0.01	0.01	0.03	0.03	0.05	0.08	1.40	0.93
Residual	4.49	0.14	0.18	0.13	0.03	0.19	0.21	0.25	0.08	0.16	—
CaO/SiO_2	—	1.00	0.98	1.03	0.97	0.95	1.07	0.85	0.65	1.03	0.99
$Al_2O_3 + MgO$	—	13.63	23.34	31.12	14.52	21.75	26.17	25.73	26.79	17.76	21.69
$(CaO + MgO)/SiO_2$[a]	—	1.01	1.21	1.52	1.22	1.20	1.30	1.14	0.88	1.20	1.20
Physical properties											
d_{50} (μm)[b]	26.812	24.35	22.73	22.29	19.67	20.35	20.85	20.40	20.11	22.75	20.94
SSA (m^2/g)[c]	0.284	0.77	0.90	0.96	1.09	0.92	0.90	0.93	1.08	0.83	0.94

Note: Bold values indidates the variation of MgO, Al_2O_3, and CaO/SiO_2 of these synthetic slags.

[a] European standard EN 15167-1 (CEN 2006) recommends that the ratio should be greater than 1.

[b] Particle size distribution of slag and quartz was measured by EyeTech, Ankersmid. The d_{50} of quartz was 24.21 μm.

[c] Specific surface area of these slags was measured by nitrogen adsorption with the Brunauer-Emmerit-Teller (BET) method.

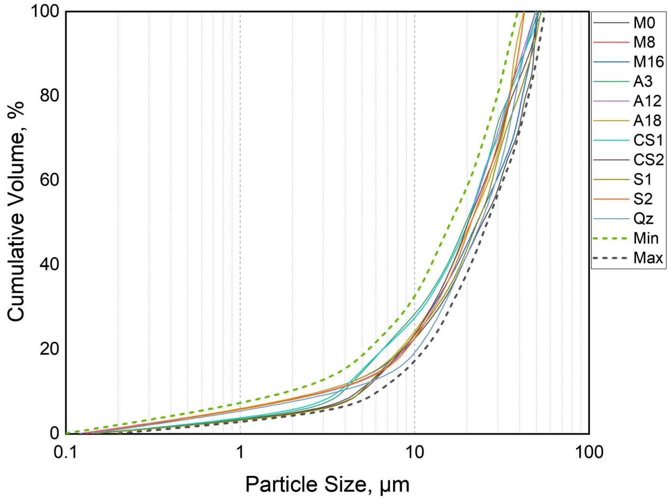

Fig. 1. Particle size distribution of slag and quartz.

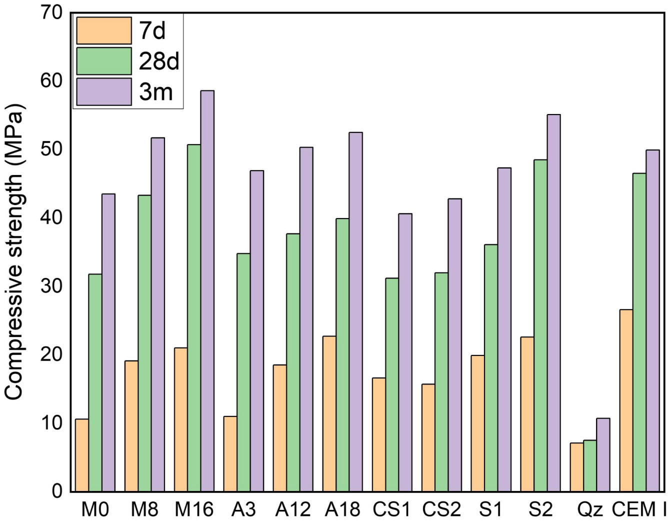

Fig. 2. Compressive strength development of slag cement pastes (MPa).

degree of slag in each system with time. For each measurement, ~0.25 g of dry sample powder (<63 μm) after hydration stop was added to the solution.

The mercury intrusion porosimeter analysis was performed with a Micromeritics Autopore IV, which determined the pore size down to 7 nm (corresponding to a 0–210 MPa range of applied pressure). After hydration stop, crushed particles were stored in a desiccator under vacuum until constant weight. Note that the surface tension of 0.485 N/m and the contact angle of 140° were utilized for determining pore size in this paper.

Slices of selected specimens were prepared for scanning electron microscopy (SEM) investigation. They were first impregnated with epoxy resin, ground with #320, #800, and #1,200 SiC grinding papers, polished down to 0.25 μm, and then carbon coated. For backscattered secondary electron (BSE) images, these carbon-coated samples were examined with a FEI Quanta FEG 650 under a 10 kV accelerating voltage and a working distance of 10 mm. X-ray energy dispersive detector was also equipped to determine the elemental compositions of phases interested with internal standard (standardless microanalysis).

Results

Compressive Strength

Fig. 2 gives the compressive strength of slag-rich cement paste up to 90 days. Commercial slags S1 and S2 showed relatively high compressive strength at 7 days in the cement paste. Slags M16 and A18 presented the highest compressive strength at early age among all synthetic slags; however, the strength development of Slag A18 at later age was inferior to Slag M16. Although with significantly lower CaO/SiO_2 ratio, Slags CS1 and CS2 displayed higher compressive strength than that of Slags M0 and A3 at early age. As can be seen, the lowest compressive strength was reached among Slags M0, A3, CS1, and CS2 mixtures at 90 days.

Kinetics of Hydration

Heat of Hydration

Fig. 3(a) shows the heat evolution rate (per gram cement) of representative cement-slag and quartz blends. The trend was overall similar among these blends. After contact with water, an initial peak occurred immediately, which can be ascribed to the wetting and dissolution of raw materials (C_3A, i.e., $3CaO \cdot Al_2O_3$ in particular). Then, the curve was dominated by the main peak (labeled as Peak I) before one day, due to the hydration of C_3S ($3CaO \cdot SiO_2$) in cement clinker, and followed by a shoulder (Peak II), indicative of the secondary aluminate reaction upon sulfate depletion. Compared with cement-quartz system, an increase in the intensity of main peak and shoulder was noted for cement-slag system. This difference was likely connected with slag dissolution, as these slags and quartz had similar physical properties, including particle size distribution and specific surface area (Table 1). In Al_2O_3-containing slag cement paste, additional Al^{3+} ions would be dissolved from slag and enter the pore solution, leading to a quicker and more intensified aluminate reaction with sulfate (Zhang et al. 2022c). In Slag M16 and A18 mixtures, the shoulders even superimposed the main peak, resulting in much more intensified and sharp peaks.

After one day, the hump (Peak III) separated the mixtures containing slags and quartz. This hump corresponded to the pozzolanic reaction between portlandite and slag. Besides, a continuous and steady hump (Peak IV) characterizing the transformation from ettringite to monosulfate was also observed after 2 days.

Fig. 3(b) reveals the cumulative heat release (per gram cement). The substitution of slag resulted in an increase in total heat release when compared to quartz. Curves deviated from each other after 1 day when slag started to react with portlandite. Al_2O_3-rich A18 and MgO-rich M16 slag blends evolved the most heat among all synthetic slag cement pastes. Commercial slag S1 and S2 blends also presented relatively high cumulative heat release. Meanwhile, although presenting a low CaO/SiO_2 ratio, CS1 and CS2 slag blends showed a similar hydration rate and total heat release to Slags M0, M8, A3, and A12.

Chemically Bound Water and Portlandite Contents

For chemically bound water (BW), it can be calculated from TG results and corrected for the water bound in portlandite (Snellings et al. 2019):

$$BW = \left(\frac{W_{50} - W_{550} - W_{H_2O\,CH}}{W_{550}}\right)$$

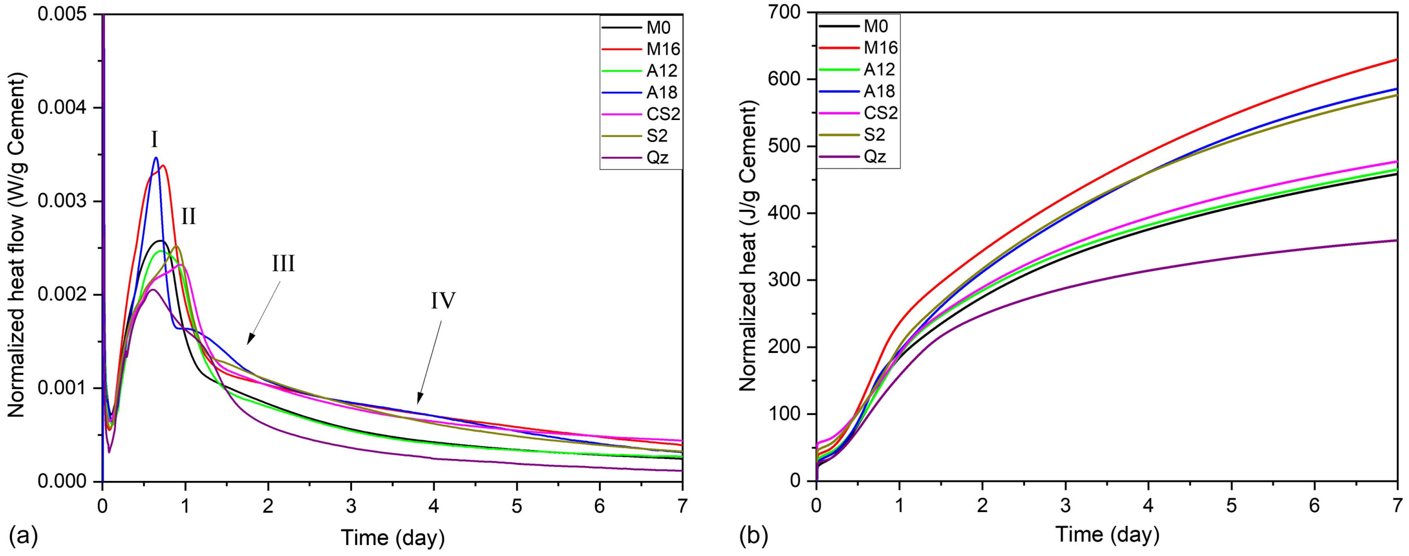

Fig. 3. (a) Heat flow as a function of time in calorimetric measurement for representative cement-slag and quartz pastes; and (b) total heat released as a function of time in calorimetric measurement for representative cement-slag and quartz pastes.

with W_{50} = sample weight at 50°C; W_{550} = sample weight at 550°C; and $W_{H_2O\,CH}$ = mass loss from the dehydroxylation of portlandite by tangent method.

At all investigated ages, M16 and A18 slag mixtures presented the most bound water contents (more than 0.16 g/g binder at 90 days). The other mixtures showed a similar value, varying from 0.10 to 0.14 after 3 months of curing. Moreover, it was found that Al_2O_3-rich slag systems, e.g., A18 (18.19% by weight), CS1 (14.51% by weight), and CS2 (17.12% by weight) blends exhibited extreme high bound water content at 7 days; however, the increment was limited up to 3 months. Taking Slag A12 as a reference, the increment was 0.064 from 7 days to 3 months, while this value was 0.045 for Slag A18, 0.020 for Slag CS1, and 0.034 for Slag CS2.

Fig. 4(b) presents the amount of portlandite remained in the blended mixture with the extension of curing age. Generally, it showed an adverse trend compared to chemically bound water content and decreased continuously because of pozzolanic reaction. Slag M16 and A18 systems exhibited the least portlandite content, and the rest varied from 0.015 to 0.035 at 90 days.

Selective Dissolution

As introduced in Kocaba et al. (2012), the slag hydration degree (α) can be determined by comparing the residues after selective dissolution of unhydrated raw material (R_u) and hydrated sample powder (R_h) through the following equation:

$$\alpha = \frac{R_u - R_h}{R_u}$$

Additionally, a correction considering that Mg^{2+} ion dissolved from slag all contributed to the formation of hydrotalcite-like phase was proposed by Luke and Glasser (1987):

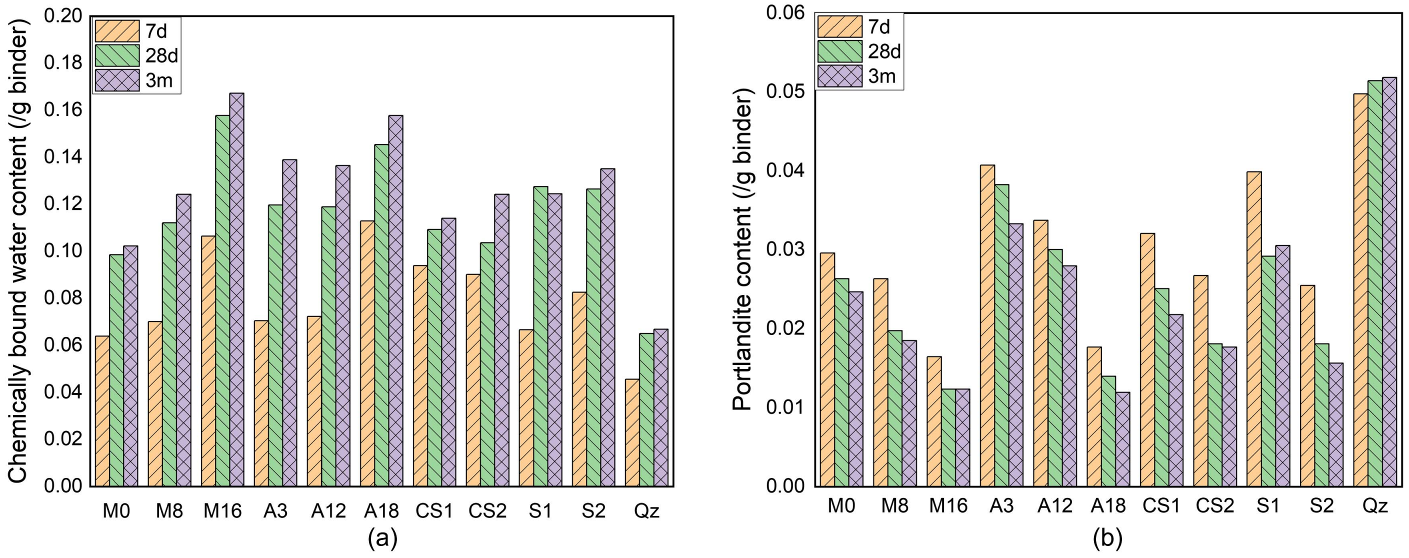

Fig. 4. (a) Chemically bound water contents; and (b) portlandite contents of cement-slag and quartz mixtures.

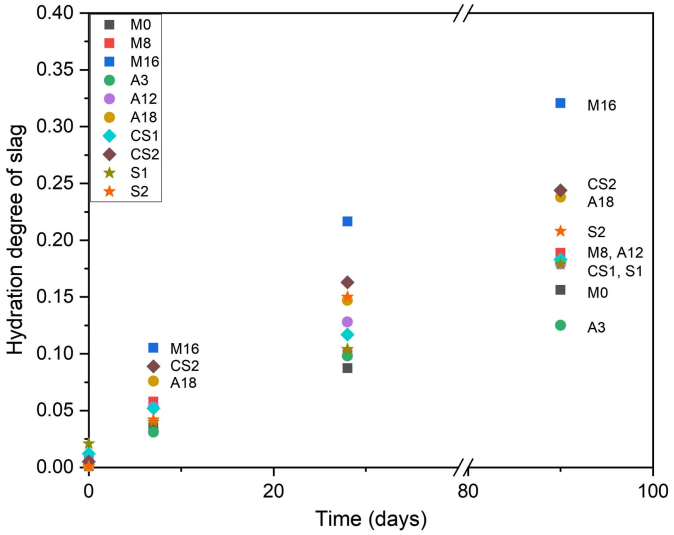

Fig. 5. Hydration degree of slag with respect to time based on selective dissolution method.

$$\alpha_{\text{correction}} = \frac{R_u - R_h}{R_u \times (1 - hM)}$$

where $h = 2.35$, indicative of the mass of hydrotalcite-like phase formed from 1 g of MgO in slag; and M = MgO content of slag (% by weight).

Fig. 5 reports the slag hydration degree of each mixture with time. Basically, the data indicated that with the increasing Al_2O_3 and/or MgO contents in slag, the hydration degree of slag increased (For Al_2O_3, A3 < M8, A12, CS1, S1, S2 < A18 and CS2. For MgO, M0 < M8, A12, CS1, S1, S2 < M16). At 90 days, the hydration degree of Slag A3 was a little more than 10%, while it exceeded 30% for Slag M16. It was also noticed that Slags M16, CS2, and A18 exhibited a slighter higher hydration degree at 7 days; however, the gap between Slag M16 and others became wider with time, and it stood out solely after 3 months. As for Slags M0 and A3, their hydration degrees were among the lowest in these mixtures at all investigated ages.

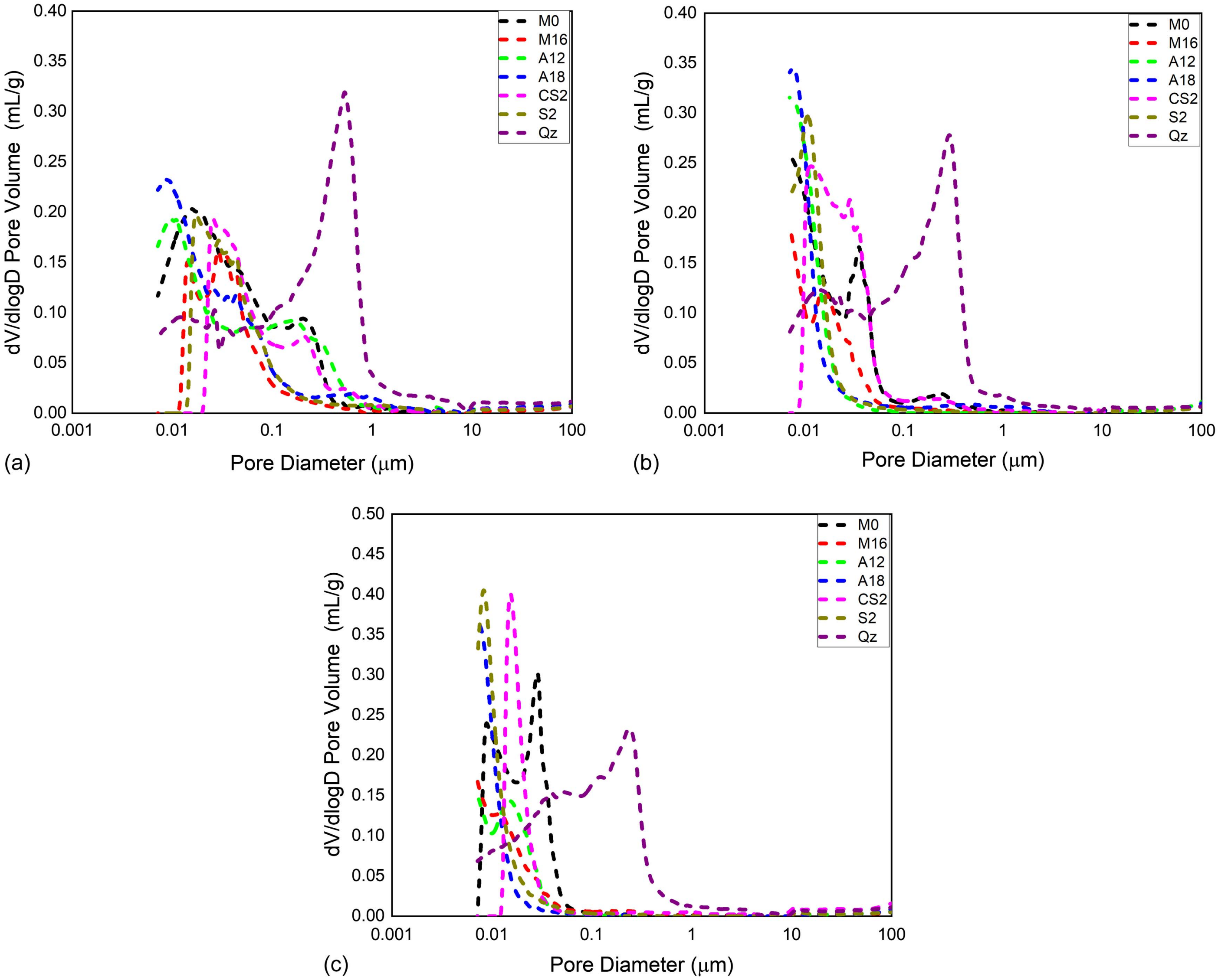

Fig. 6. Differential pore size distribution of representative cement-slag and quartz pastes measured at (a) 7 days; (b) 28 days; and (c) 90 days.

Table 3. Critical pore diameter of each mixture based on MIP analysis

	Critical pore diameter (nm)		
Slag	7 days	28 days	3 months
M0	18.13/205.47	—/36.28	8.44/29.45
M8	19.42/47.84	—/29.45	9.69
M16	13.72/29.46	—/15.75	—
A3	11.94/236.14	—/29.46	9.04/22.29
A12	10.39/178.49	7.83	—/14.70
A18	9.04/44.56	7.83	—
CS1	16.89/205.47	9.69/36.24	11.13
CS2	25.61/205.65	9.69/29.46	14.71
S1	8.44/29.46	11.94	11.13
S2	16.89/44.55	11.13	8.44
Qz	542.09	13.72/311.85	38.79/236.01

Pore Structure

Fig. 6 exhibits the differential pore size distribution of representative cement-slag and quartz pastes at all investigated time. Table 3 summarizes the critical pore diameter of systems. It was found that hydrates produced from pozzolanic reaction were beneficial for the densification of pore structure. The critical pore radius reduced with the extended curing time. At 7 days, all pastes exhibited a bimodal pore structure, and most of them evolved into a unimodal one eventually at different ages, e.g., 28 days for Slag S2 paste and 90 days for Slag CS2 paste (Table 3). For Slag M0 and A3 pastes, the bimodal pore structure was remained even after 3 months of curing although the critical pore radius decreased considerably. Meanwhile, note that the critical pore diameter decreased notably with increasing Al_2O_3 and/or MgO contents in slag. Commercial slag S1 and S2 blends showed a comparable pore structure at 90 days to Slag M8, A12, CS1, and CS2 systems.

Hydration Products

Solid Phases

For a clear view, TG and derivative thermogravimetric (DTG) results of representative pastes at specific ages are displayed in Figs. 7(a and b), respectively. Overall, the hydration products precipitated in each mixture were identical. The distinct peak at 400°C–500°C can be assigned to the dehydroxylation of $Ca(OH)_2$. The peak at ~350°C and the shoulder at ~250°C implied the presence of hydrotalcite-like phase as the secondary hydrate of slag. Thus, it was not observed in the blend of slag M0 and quartz. The mass loss for ettringite and C─S─H gel phase overlapped at 100°C–150°C. The shoulder at about 200°C implied the precipitation of monosulfate. Slags M16, A18, and CS2 with the highest Al_2O_3 contents presented the most monosulfate in the mixtures at 7 days.

Similarly, the typical XRD results are present in Fig. 8. The peaks for portlandite, unhydrated C_3S, and C_2S at specific ages were clearly visible. The main peak of C─S─H gel phase (low crystallinity) was located at around ($2\theta =$) 30°, which was very difficult to distinguish it from that of C_3S. Note that the peak intensity of $Ca(OH)_2$ reduced continuously with time because of the pozzolanic activity of slag. Also, the most portlandite was detected in Slag M0 paste while the least in Slag M16 and A18 systems at all investigated ages.

SEM-BSE

Fig. 9 illustrates the BSE micrographs of typical specimens at 90 days. Unhydrated cement clinkers and slag grains, hydration products, and pores were detected to form the microstructure of each mixture. Unhydrated cement clinkers, appearing as the lightest parts (circled and labeled 1 in A18 mixture), were still observed after 3 months. Monosulfate existed as fine, widespread, and compact clusters intermixed with cement matrix, which are circled and labeled 2 in M16 mixture (Scrivener 2004). Hydrates precipitated as rims around unreacted slag grains were also visible.

Chemical Composition

C─S─H Gel Phase

The compositions of cement matrix and hydration rims around unreacted slag particles were determined by SEM-EDS microanalysis. Representative scatter plots of Al/Ca against Si/Ca in atomic ratio are exhibited in Fig. 10(a). Moreover, the Ca/Si and Al/Si ratios of

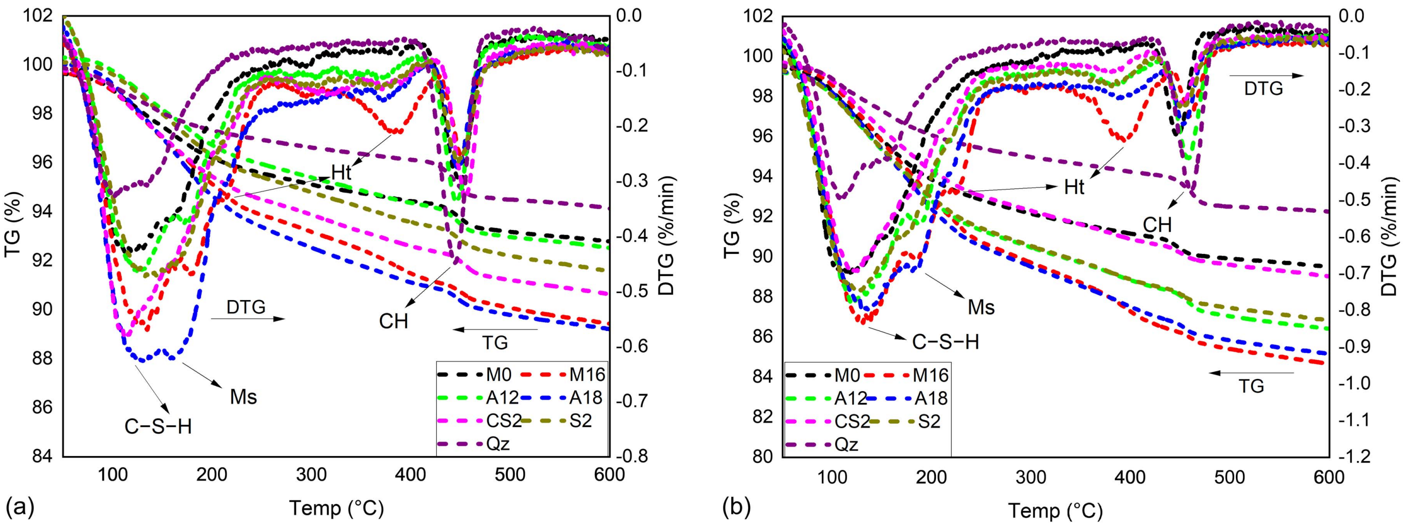

Fig. 7. Typical TG and DTG results of cement-slag and quartz mixtures after curing of (a) 7 days; and (b) 3 months. CH is portlandite, Ms is monosulfate, and Ht is hydrotalcite-like phase.

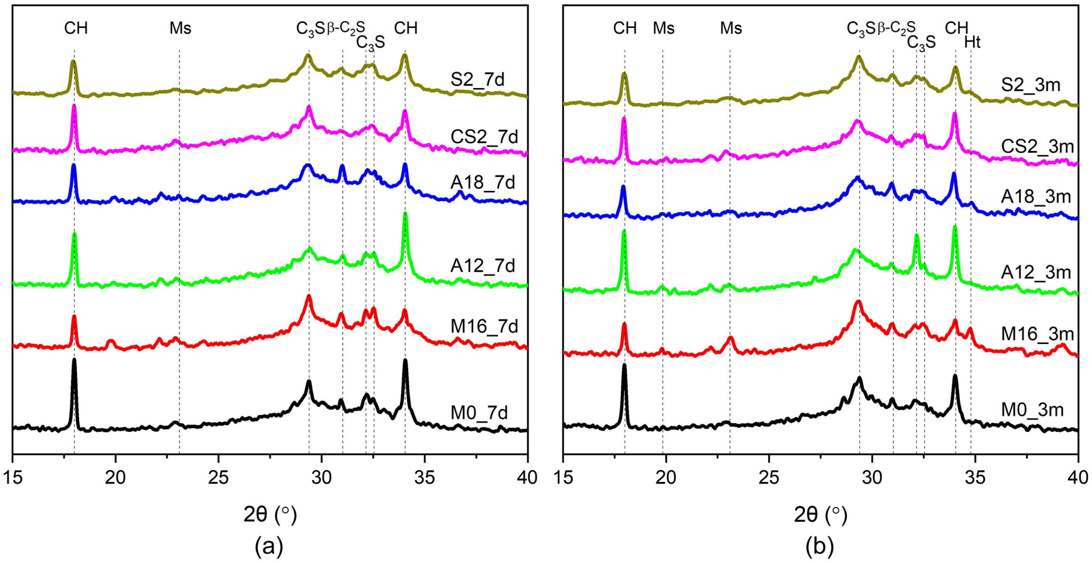

Fig. 8. XRD analysis of typical cement-slag blends after curing of (a) 7 days; and (b) 3 months. CH is portlandite, Ms is monosulfate, and Ht is hydrotalcite-like phase.

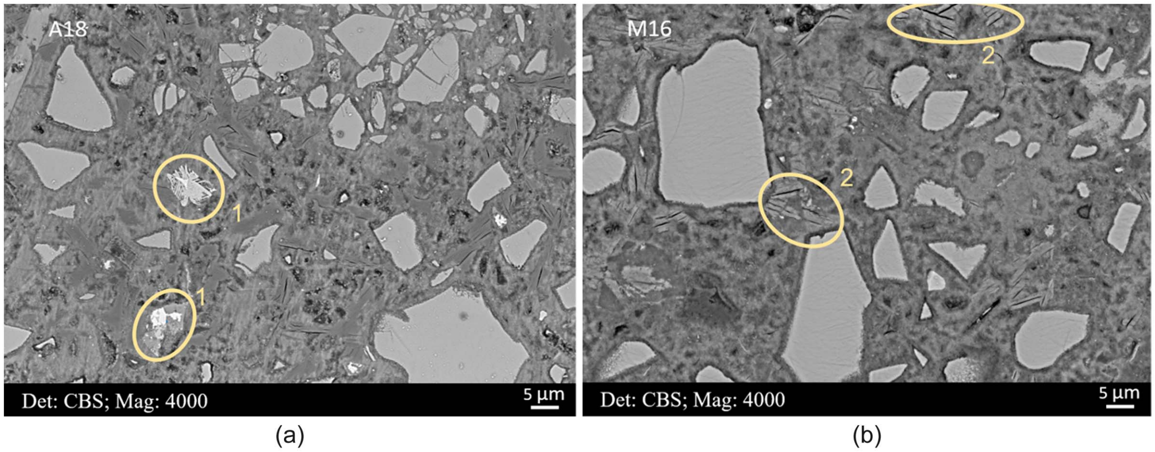

Fig. 9. Representative microstructures of slag cement paste after 3 months of curing: (a) A18; and (b) M16.

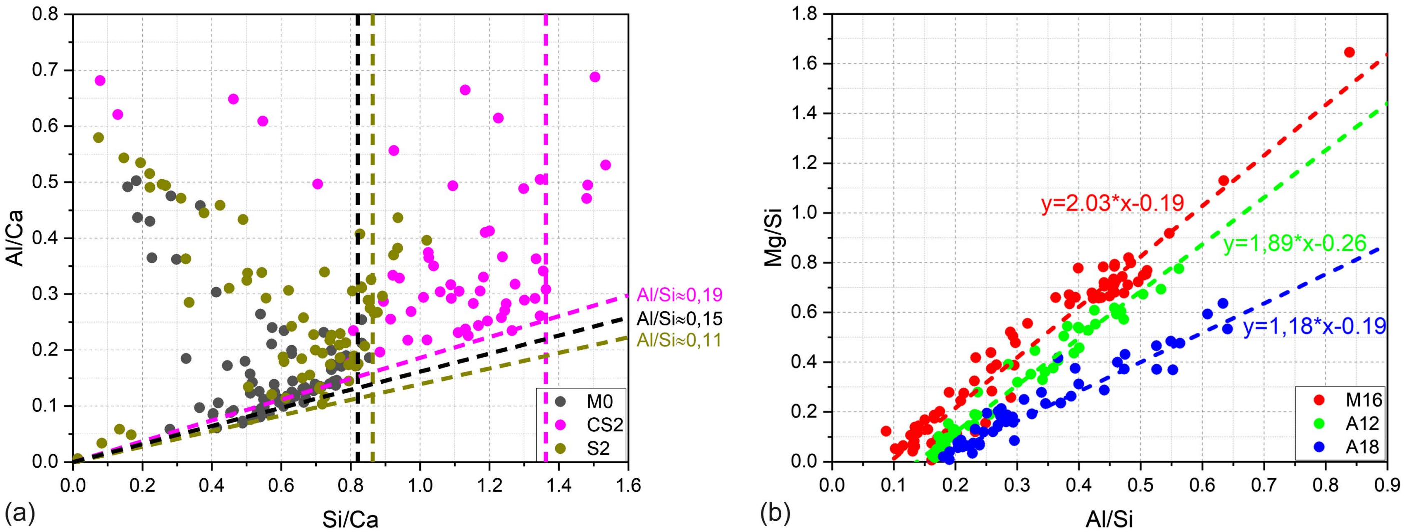

Fig. 10. Typical plots of (a) Al/Ca against Si/Ca; and (b) Mg/Si against Al/Si in atomic ratio of cement-slag system after 3 months of curing.

Table 4. Ca/Si and Al/Si atomic ratios of C—S(A)—H gel phase, and Mg/Al atomic ratio of hydrotalcite-like phase in cement-slag blends at 90 days

Ratio	M0	M8	M16	A3	A12	A18	CS1	CS2	S1	S2
Ca/Si	~1.23	~1.28	~1.32	~1.14	~1.17	~1.08	~1.02	~0.74	~1.23	~1.21
Al/Si	~0.15	~0.11	~0.11	~0.07	~0.13	~0.18	~0.15	~0.19	~0.10	~0.11
Mg/Al	—	~1.65	~2.03	~1.99	~1.89	~1.18	~1.85	~1.77	~1.72	~1.78

all mixtures are calculated [similar to the works in Deschner et al. (2012) and Whittaker et al. (2016)] and summarized in Table 4.

Generally, the Ca/Si atomic ratio measured at 90 days fluctuated from 1.0 to 1.20, except Slag CS1 and CS2 pastes [Table 4 and Fig. 10(a)]. It matched well with the values determined in Escalante-Garcia and Sharp (2004), Richardson (2004), and Taylor et al. (2010). For Slag CS1 and CS2 mixtures, the measured Ca/Si atomic ratio reduced notably owing to the Ca/Si ratio of raw slags.

Conversely, the variation of Al/Si atomic ratio appeared to be a little complicated. It was well accepted that this value was positively related to the Al_2O_3 content of slag. For example, Slags A18 and CS1 with higher Al_2O_3 contents exhibited higher Al/Si atomic ratios, while Slag A3 containing the least Al_2O_3 showed the lowest Al/Si ratio. It was consistent with the results found in Whittaker et al. (2014, 2016). Furthermore, one should keep in mind that MgO in slag also affected the release of aluminum, as part of aluminum would be attracted by magnesium to form hydrotalcite-like phase in slag rim. In Slag M16 blend, the Al/Si atomic ratio was significantly lower than that of other blends with similar Al_2O_3 contents, which was mainly attributed to the incorporation of Al^{3+} ions in the precipitation of hydrotalcite-like phase.

Hydrotalcite-Like Phase

Hydrotalcite-like phase is the primary hydrate of slag, and its Mg/Al atomic ratio is close to 2 (Taylor et al. 2010; Zhang and Çopuroğlu 2022; Zhang et al. 2022a). In the present study, the Mg/Al ratio was obtained from the slope of regression line when plotting Mg/Si versus Al/Si in molar ratio. Fig. 10(b) depicts the Mg/Si against Al/Si plots of typical slag cement pastes. Similarly, the Mg/Al ratio of all blends was also calculated and summarized in Table 4. As can be seen, hydrotalcite-like phase formed in each mixture presented a significantly different Mg/Al atomic ratio. The results in Fig. 11 demonstrates that the Mg/Al atomic ratio of hydrotalcite-like phase was positively related to the Mg/Al atomic ratio of raw slag itself. The Mg dissolved from slag cannot migrate outside into cement matrix, and it would participate into the formation of hydrotalcite-like phase in the rim.

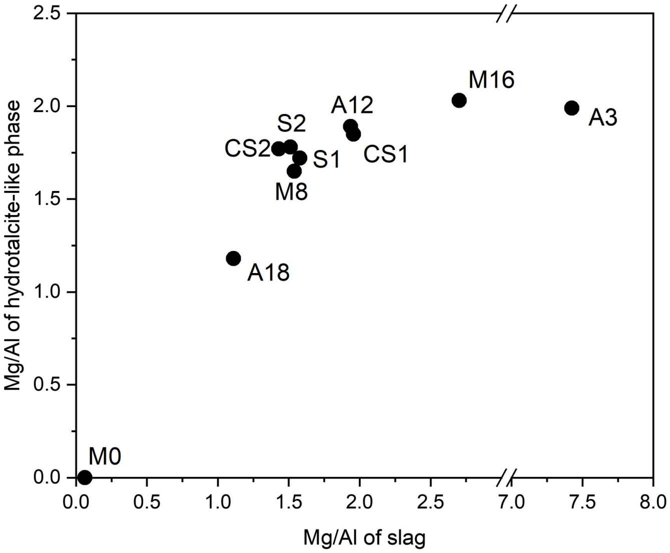

Fig. 11. Correlation between Mg/Al atomic ratio of hydrotalcite-like phase measured at 90 days and Mg/Al atomic ratio of raw slag itself.

Discussion

Influence of Al_2O_3 and MgO Contents at Early and Later Age

Slag CS2, which contained high Al_2O_3 content (17.12% by weight), was employed as an example to illustrate the influence of Al_2O_3 in slag on the performance of blended paste. Initially it should present low reactivity owing to its low CaO/SiO_2 ratio (0.65); however, Slag CS2 cement released more than 400 J/g heat during calorimetric test [Fig. 3(b)], only next to Slag M16 and A18 mixtures among all synthetic slags. Additionally, the CS2 cement-slag system contained approximately 9% chemically bound water at 7 days, only next to Slag M16, A18, and CS1 mixtures, all of which contained high Al_2O_3 contents [Fig. 4(a)]. The hydration degree of Slag CS2 in the blend was relatively high at early age, reaching ~10% (Fig. 5). Compared to the formation of C—S—H gel phase, the precipitation of Al-bearing phases (e.g., ettringite and monosulfate) was very exothermic (Blotevogel et al. 2020; Whittaker et al. 2014). It partially explained why mixtures containing Al_2O_3-rich slag released high heat during calorimetric measurement. Furthermore, the most monosulfate was found in Al_2O_3-rich slag cement paste at 7 days (Fig. 7), which incorporated more chemically bound water than C—S—H gel phase, leading to a high bound water content measured by TG. Besides, due to the higher molar volume of Al-bearing phases, they filled up pores and were beneficial for the compressive strength development (Snellings et al. 2019), which was also confirmed by the compressive strength results in the present research (Fig. 2).

However, the situation was different after 3 months of curing, and the beneficial effect of Al_2O_3 or Al-bearing phases disappeared at later age. As can be seen, the increment of chemically bound water was quite low for Slag CS2 mixture from 7 days to 3 months. It also agreed well with the development of compressive strength (Fig. 2), of which the M0, A3, and CS2 cement-slag systems presented the lowest compressive strengths among all slag-containing mixtures at later age.

As for MgO, it works as a network modifier of the glass structure (Mills et al. 2012; Xuan et al. 2018; Zhang et al. 2014). The results from selective dissolution test verified that after 3 months of curing, the hydration degree of Slag M16 stood out solely and exceeded 30%, suggested a much distorted and depolymerized network structure of slag at higher MgO mass percentage. In this paper, paste containing MgO-rich slag (e.g., Slag M16) performed well at both early and later age.

Correlation between Slag Reactivity and Properties of the Blended Cement Paste

Zhang et al. (2022d) classified the reactivity of slag with its chemical composition based on a graphic method. This method divided the defined area containing slags into regions presenting *similar performance* and demonstrated the interaction among main metal oxides directly. In the present paper, we would also like to utilize this coordinate system of $(CaO/SiO_2)-(Al_2O_3 + MgO)$ in weight percentage (based on slag chemistry) to classify the properties of slag cement paste.

The distribution of synthetic and commercial slags in $(CaO/SiO_2)-(Al_2O_3 + MgO)$ coordinate system is illustrated in Fig. 12. Based on the results of different characterization methods, the whole coordinate area can be further divided into three regions roughly following: $Al_2O_3 + MgO < 15\%$ by weight (Region I), $15 < Al_2O_3 + MgO < 25\%$ by weight (Region II), and $Al_2O_3 + MgO > 25\%$ by weight (Region III). Region I consisted of Slags M0 and A3, which presented the poorest properties of the corresponding slag cement pastes. Region III involved Slags M16 and A18, and these two slag cement pastes performed the best among all slags investigated although Slag A18 paste was inferior to Slag M16 paste at later age. The remaining slags were located at Region II, which showed similar and moderate performance in cement paste.

Synthetic slag CS1 and CS2 cement pastes displayed significantly different performance at early and later age. At early age, the negative effect of decreasing CaO/SiO_2 ratio on reactivity was compensated by high Al_2O_3 and/or MgO contents in slag. As present by compressive strength, chemically bound water, hydration degree, etc., slag CS1 and CS2 pastes showed comparative performance with respect to Slag M8 and A12 pastes and could be classified into Region II. However, at later age when the beneficial effect of Al_2O_3 vanished, Slag CS1 and CS2 pastes only exhibited comparative properties to Slag M0 and A3 blends, and was grouped into Region I.

Zhang et al. (2022b) also addressed the role of element sulfur existing in commercial slag. It was noted that the sulfur started to participate in the hydration process after one day while its influence became negligible at 90 days in cement-slag system. In this paper, commercial Slag S1 and S2 blends presented relatively high cumulative heat release during calorimetric measurement (Fig. 3) and compressive strength at 7 days (Fig. 2). However, their performance was only similar to Slag M8 and A12 mixtures at later age, confirming that the positive effect of sulfur also disappeared at later age.

Additionally, note that there was no slag located at the slash line region (Fig. 12), characterized by $CaO/SiO_2 > 1.1$ and $15 < Al_2O_3 + MgO < 25\%$ by weight. This region was separated specifically as there was a trend for consistent production of lime-rich slag in steelmaking manufacturing, which appeared to be especially distinct across Europe (Alonso et al. 2019; Dai et al. 2021; Kiiashko et al. 2021; Ukpata et al. 2019), North America (Burciaga-Díaz 2019; Sakr and Bassuoni 2021; Wang et al. 2020), and Australia (Samarakoon et al. 2020) according to a survey on the recent publications (2019–2021). It deserves further research in the future that whether this continuous increasing in CaO content in slag can enhance the properties of slag cement paste to the level of Slag M16 and A18 mixtures.

When comparing the $(CaO/SiO_2)-(Al_2O_3 + MgO)$ coordinate system used to estimate slag reactivity [Fig. 14(b) in Zhang et al. (2022d)] and the properties of slag cement paste in the present study (Fig. 12), attention should be paid to the aluminum- and sulfur-rich slag. Aluminum and sulfur dissolved from slag participate into the formation of ettringite and/or monosulfate, resulting in more heat release, chemical water binding, and space filling, which can be characterized by different methods and thus lead to a good estimation of slag reactivity and good performance of slag cement paste at early age. However, the positive effect of aluminum and sulfur disappears at later age. It can be fundamentally ascribed to the role of them in the network structure of slag. Different from network modifier (e.g., Ca and Mg), aluminum and sulfur are intermediates, and cannot decrease the polymerization degree of glass network structure.

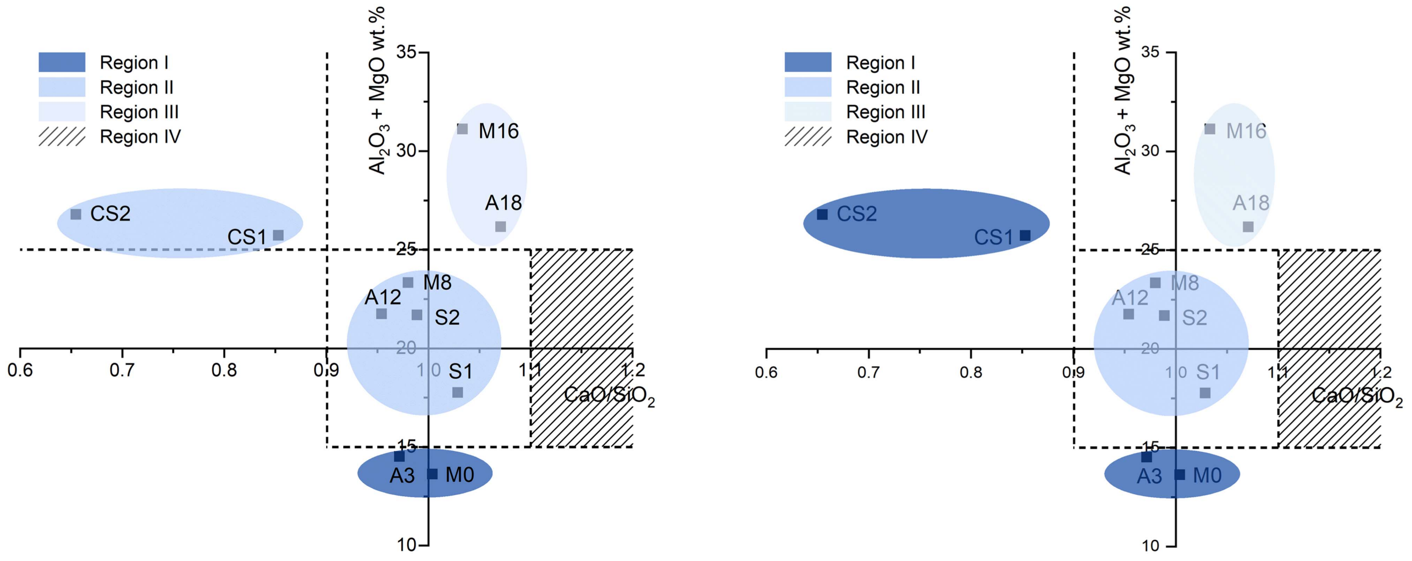

(a)

(b)

Fig. 12. Distribution of slag in $(CaO/SiO_2)-(Al_2O_3 + MgO)$ coordinate system in weight percentage and the corresponding classification of properties of slag cement paste: (a) early age; and (b) later age. Region I shows poor properties, Region II shows moderate properties, and Region III shows good properties.

Conclusions

This study provided important insight regarding the influence of slag chemistry on the early and later age properties of slag-rich cement paste. In addition, the correlation between slag reactivity and properties of slag cement paste was discussed. The main conclusions were as follows:

- Cement paste containing aluminum/sulfur-rich slag performed better at early age as it favored the formation of ettringite and/or monosulfate. However, the positive effect of aluminum disappeared at later age.
- MgO effectively favored the formation of hydrotalcite-like phase. MgO-rich slag paste performed extremely well at both early and later ages. It was also noted that the Mg/Al atomic ratio of hydrotalcite-like phase measured at 90 days was positively related to the Mg/Al atomic ratio of raw slag itself. Conversely, with the increasing MgO content in slag, the Al/Si atomic ratio of C─S(A)─H gel phase decreased.
- Synthetic slag CS1 and CS2 mixtures presented significantly different performance at early and later ages. High Al_2O_3 and/or MgO contents can compensate the negative effect of reduced CaO/SiO_2 ratio at early age while not at later age. They only showed a comparative performance to slag M0 and A3 systems at later age, the poorest properties among all mixtures investigated.

Data Availability Statement

Some or all data that support the findings of this study are available from the corresponding author upon reasonable request.

Acknowledgments

Authors thank Arjan Thijssen (Microlab, TU Delft) for his technical support. Jeanette van den Bos (BAM Infraconsult B.V.) and René Albers (Ecocem Benelux B.V.) are gratefully acknowledged for the technical discussions and providing commercial slags.

References

Alonso, M. M., C. Gascó, M. M. Morales, J. A. Suárez-Navarro, M. Zamorano, and F. Puertas. 2019. "Olive biomass ash as an alternative activator in geopolymer formation: A study of strength, radiology and leaching behavior." *Cem. Concr. Compos.* 104 (Nov): 103384. https://doi.org/10.1016/j.cemconcomp.2019.103384.

Blotevogel, S., A. Ehrenberg, L. Steger, L. Doussang, J. Kaknics, C. Patapy, and M. Cyr. 2020. "Ability of the R3 test to evaluate differences in early age reactivity of 16 industrial ground granulated blast furnace slags (GGBS)." *Cem. Concr. Res.* 130 (Apr): 105998. https://doi.org/10.1016/j.cemconres.2020.105998.

Bougara, A., C. Lynsdale, and N. B. Milestone. 2010. "Reactivity and performance of blastfurnace slags of differing origin." *Cem. Concr. Compos.* 32 (4): 319–324. https://doi.org/10.1016/j.cemconcomp.2009.12.002.

Burciaga-Díaz, O. 2019. "Parameters affecting the properties and microstructure of quicklime (CaO)-activated slag cement pastes." *Cem. Concr. Compos.* 103 (Oct): 104–111. https://doi.org/10.1016/j.cemconcomp.2019.05.002.

CEN (European Committee for Standardization). 2006. *Ground granulated blast furnace slag for use in concrete, mortar and grout—Part 1: Definitions, specifications and conformity criteria*. EN 15167-1:2006. Brussels, Belgium: CEN.

CEN (European Committee for Standardization). 2016. *Methods of testing cement—Part 1: Determination of strength*. EN-196-1:2016. Brussels, Belgium: CEN.

Chen, W., and H. Brouwers. 2007. "The hydration of slag. Part 2: Reaction models for blended cement." *J. Mater. Sci.* 42 (2): 444–464. https://doi.org/10.1007/s10853-006-0874-1.

Dai, X. D., S. Aydin, M. Y. Yardimci, R. E. N. Qiang, K. Lesage, and G. D. Schutter. 2021. "Rheology, early-age hydration and microstructure of alkali-activated GGBFS-fly ash-limestone mixtures." *Cem. Concr. Compos.* 124 (Nov): 104244. https://doi.org/10.1016/j.cemconcomp.2021.104244.

Deschner, F., F. Winnefeld, B. Lothenbach, S. Seufert, P. Schwesig, S. Dittrich, F. Goetz-Neunhoeffer, and J. Neubauer. 2012. "Hydration of portland cement with high replacement by siliceous fly ash." *Cem. Concr. Res.* 42 (10): 1389–1400. https://doi.org/10.1016/j.cemconres.2012.06.009.

Escalante-Garcia, J. I., and J. Sharp. 2004. "The chemical composition and microstructure of hydration products in blended cements." *Cem. Concr. Compos.* 26 (8): 967–976. https://doi.org/10.1016/j.cemconcomp.2004.02.036.

Juenger, M. C., R. Snellings, and S. A. Bernal. 2019. "Supplementary cementitious materials: New sources, characterization, and performance insights." *Cem. Concr. Res.* 122 (Aug): 257–273. https://doi.org/10.1016/j.cemconres.2019.05.008.

Kiiashko, A., M. Chaouche, and L. Frouin. 2021. "Effect of phosphonate addition on sodium carbonate activated slag properties." *Cem. Concr. Compos.* 119 (May): 103986. https://doi.org/10.1016/j.cemconcomp.2021.103986.

Kocaba, V., E. Gallucci, and K. L. Scrivener. 2012. "Methods for determination of degree of reaction of slag in blended cement pastes." *Cem. Concr. Res.* 42 (3): 511–525. https://doi.org/10.1016/j.cemconres.2011.11.010.

Kucharczyk, S., M. Zajac, C. Stabler, and R. M. Thomsen. 2019. "Structure and reactivity of synthetic CaO-Al_2O_3-SiO_2 glasses." Accessed June 1, 2019. https://www.sciencedirect.com/author/55663279100/mohsen-ben-haha.

Li, Y., Y. Liu, X. Z. Gong, Z. R. Nie, S. P. Cui, Z. H. Wang, and W. J. Chen. 2016. "Environmental impact analysis of blast furnace slag applied to ordinary portland cement production." *J. Cleaner Prod.* 120 (May): 221–230. https://doi.org/10.1016/j.jclepro.2015.12.071.

Luke, K., and F. P. Glasser. 1987. "Selective dissolution of hydrated blast furnace slag cements." *Cem. Concr. Res.* 17 (2): 273–282. https://doi.org/10.1016/0008-8846(87)90110-4.

Mills, K. C., L. Yuan, Z. Li, G. H. Zhang, and K. C. Chou. 2012. "A review of the factors affecting the thermophysical properties of silicate slags." *High Temp. Mater. Processes* 31 (4–5): 301–321. https://doi.org/10.1515/htmp-2012-0097.

Özbay, E., M. Erdemir, and H. İ. Durmuş. 2016. "Utilization and efficiency of ground granulated blast furnace slag on concrete properties—A review." *Constr. Build. Mater.* 105 (Feb): 423–434. https://doi.org/10.1016/j.conbuildmat.2015.12.153.

Richardson, I. G. 2004. "Tobermorite/jennite-and tobermorite/calcium hydroxide-based models for the structure of CSH: Applicability to hardened pastes of tricalcium silicate, β-dicalcium silicate, portland cement, and blends of portland cement with blast-furnace slag, metakaolin, or silica fume." *Cem. Concr. Res.* 34 (9): 1733–1777. https://doi.org/10.1016/j.cemconres.2004.05.034.

Sakr, M., and M. Bassuoni. 2021. "Performance of concrete under accelerated physical salt attack and carbonation." *Cem. Concr. Res.* 141 (Mar): 106324. https://doi.org/10.1016/j.cemconres.2020.106324.

Samarakoon, M. H., P. G. Ranjith, W. H. Duan, and V. R. S. De Silva. 2020. "Properties of one-part fly ash/slag-based binders activated by thermally-treated waste glass/NaOH blends: A comparative study." *Cem. Concr. Compos.* 112 (Sep): 103679. https://doi.org/10.1016/j.cemconcomp.2020.103679.

Schöler, A., F. Winnefeld, M. B. Haha, and B. Lothenbach. 2017. "The effect of glass composition on the reactivity of synthetic glasses." *J. Am. Ceram. Soc.* 100 (6): 2553–2567. https://doi.org/10.1111/jace.14759.

Scrivener, K. L. 2004. "Backscattered electron imaging of cementitious microstructures: Understanding and quantification." *Cem. Concr. Compos.* 26 (8): 935–945. https://doi.org/10.1016/j.cemconcomp.2004.02.029.

Snellings, R., X. R. Li, F. Avet, and K. Scrivener. 2019. "Rapid, robust, and relevant (R3) reactivity test for supplementary cementitious materials." *ACI Mater. J.* 116 (4): 155–162. https://doi.org/10.14359/51716719.

Sohn, I., and D. J. Min. 2012. "A review of the relationship between viscosity and the structure of calcium-silicate-based slags in ironmaking." *Steel Res. Int.* 83 (7): 611–630. https://doi.org/10.1002/srin.201200040.

Taylor, H. F. 1997. *Cement chemistry (Vol. 2)*. London: Thomas Telford.

Taylor, R., I. Richardson, and R. Brydson. 2010. "Composition and microstructure of 20-year-old ordinary portland cement–ground granulated blast-furnace slag blends containing 0 to 100% slag." *Cem. Concr. Res.* 40 (7): 971–983. https://doi.org/10.1016/j.cemconres.2010.02.012.

Ukpata, J. O., P. M. Basheer, and L. Black. 2019. "Expansion of CEM I and slag-blended cement mortars exposed to combined chloride-sulphate environments." *Cem. Concr. Res.* 123 (Sep): 105794. https://doi.org/10.1016/j.cemconres.2019.105794.

Wang, S. Y., E. McCaslin, and C. E. White. 2020. "Effects of magnesium content and carbonation on the multiscale pore structure of alkali-activated slags." *Cem. Concr. Res.* 130 (Apr): 105979. https://doi.org/10.1016/j.cemconres.2020.105979.

Whittaker, M., M. Zajac, M. B. Haha, and L. Black. 2016. "The impact of alumina availability on sulfate resistance of slag composite cements." *Constr. Build. Mater.* 119 (Aug): 356–369. https://doi.org/10.1016/j.conbuildmat.2016.05.015.

Whittaker, M., M. Zajac, M. B. Haha, F. Bullerjahn, and L. Black. 2014. "The role of the alumina content of slag, plus the presence of additional sulfate on the hydration and microstructure of portland cement-slag blends." *Cem. Concr. Res.* 66 (Dec): 91–101. https://doi.org/10.1016/j.cemconres.2014.07.018.

Xuan, W., J. Zhang, and D. Xia. 2018. "The influence of MgO on the crystallization characteristics of synthetic coal slags." *Fuel* 222 (Jun): 523–528. https://doi.org/10.1016/j.fuel.2018.02.197.

Yang, Y., K. Raipala, and L. Holappa. 2014. "Ironmaking." *Treatise Process Metall.* 3 (Apr): 2–88. https://doi.org/10.1016/B978-0-08-096988-6.00017-1.

Zhang, S. F., X. Zhang, W. L. Lv, C. G. Bai, and L. Wang. 2014. "Relationship between structure and viscosity of $CaO-SiO_2-Al_2O_3-MgO-TiO_2$ slag." *J. Non-Cryst. Solids* 402 (Oct): 214–222. https://doi.org/10.1016/j.jnoncrysol.2014.06.006.

Zhang, Y., and O. Çopuroğlu. 2022. "The role of hydrotalcite-like phase and monosulfate in slag cement paste during atmospheric and accelerated carbonation." *Cem. Concr. Compos.* 132 (Sep): 104642. https://doi.org/10.1016/j.cemconcomp.2022.104642.

Zhang, Y., M. F. Liang, Y. D. Gan, and O. Çopuroğlu. 2022a. "Effect of MgO content on the quantitative role of hydrotalcite-like phase in a cement-slag system during carbonation." *Cem. Concr. Compos.* 134 (Nov): 104765. https://doi.org/10.1016/j.cemconcomp.2022.104765.

Zhang, Y., E. Schlangen, and O. Çopuroğlu. 2022b. "Effect of slags of different origins and the role of sulfur in slag on the hydration characteristics of cement-slag systems." *Constr. Build. Mater.* 316 (Jan): 125266. https://doi.org/10.1016/j.conbuildmat.2021.125266.

Zhang, Y., Z. Wan, L. M. de Lima Junior, and O. Çopuroğlu. 2022c. "Early age hydration of model slag cement: Interaction among C_3S, gypsum and slag with different Al_2O_3 contents." *Cem. Concr. Res.* 161 (Aug): 106954. https://doi.org/10.1016/j.cemconres.2022.106954.

Zhang, Y., S. Z. Zhang, Y. Chen, and O. Çopuroğlu. 2022d. "The effect of slag chemistry on the reactivity of synthetic and commercial slags." *Constr. Build. Mater.* 335 (Jun): 127493. https://doi.org/10.1016/j.conbuildmat.2022.127493.